Journal Name

ARTICLE

Low Dimensional and Frustrated Antiferromagnetic Interactions in Transition Metal Chloride Complexes with Simple Amine Ligands

Received 00th January 20xx,
Accepted 00th January 20xx

DOI: 10.1039/x0xx00000x

www.rsc.org/

James E. Chalmers, [a] Anant Kumar Srivastava,[a] Richard J. C. Dixey,[a] Krrishna Sivakumaran[a] and Paul J. Saines*[a]

This study reports the facile synthesis, crystal structures and magnetic properties of five new Mn, Co and Cu complexes with chloride and simple amine ligands. The four hydrazinium complexes are discrete in nature while the O-methylhydroxylamine phase contains edge-sharing chains bridged by chloride ligands. Investigation of the magnetic properties of these materials reveals that two of these materials, $Co(NH_3NH_2)_2(H_2O)_2Cl_4$ and $Cu(NH_2OCH_3)_2Cl_2$, exhibit interesting antiferromagnetic properties arising from their low dimensional structures. $Co(NH_3NH_2)_2(H_2O)_2Cl_4$ appears to exhibit significant 2D magnetic frustration while the magnetic susceptibilities of $Cu(NH_2OCH_3)_2Cl_2$ are well fitted by a one-dimensional chain model. The relationship between the strength of the magnetic coupling observed in these materials and their likely exchange pathways are also discussed.

1. Introduction

Low-dimensional magnets have attracted sustained interest for their ability to host unconventional physics, as reflected by the award of the 2016 Nobel prize to Haldane for his theorectical work in this area.[1, 2] This includes magnetic chains, which can support spinon quasi-particles that fractionalise electrons by carrying their spin but not charge.[1] Magnetic sheets, on the other hand, provide the basis for triangular and Kagome arrangements of cations whose conflicting antiferromagnetic interactions cannot be mutually satisfied.[3] This gives rise to magnetic frustration, resulting in exotic states. Experimentally achieving systems with strong magnetic coupling in one or two dimensions remains difficult, particularly in close packed oxides that have traditionally attracted the most attention in the field of magnetism as even canonical systems, e.g. $Ca_3Co_2O_6$,[4] typically have significant residual coupling between their low dimensional units. Systems incorporating organic building blocks that act as spacers between inorganic chains and sheets built from magnetic cations have, however, been shown to be a successful way of achieving phases which host a variety of isolated magnetic chains, ladders and sheets.[5-8]

Much of the interest in magnetic systems built from combining organic and inorganic building blocks centres on coordination frameworks, including dense metal-organic frameworks (MOFs) where organic linkers connect neighbouring magnetic metal centres mediating magnetic coupling between these.[5, 9] Conversely in other compounds, such as the versatile A_2MX_4 (where A is typically a monovalent N-containing organic cation, M is a divalent transition metal and X is a halide) family, magnetic coupling between discrete transition metal complexes is mediated through short X…X contacts under 4 Å with the organic building block simply acting as a spacer and not coordinating to the transition metal.[6-8, 10, 11] In light of the significant interest in these distinct groups of compounds, it is interesting to explore what new low dimensional magnetic architectures can be achieved by compounds related to the A_2MX_4 phases, with regards to having short X…X contacts capable of facilitating magnetic coupling but with organic components that prefer to coordinate to one transition metal rather than act simply in a space filling role. Hydrazine and O-methylhydroxylamine are two of the simplest amines with a tendency to coordinate to a transition metal centre, but only two complexes containing both these and halide ligands have been reported thus far, neither of whose magnetic properties have been explored.[12]

In this paper, we report five new complexes with O-methylhydroxylamine or hydrazinium molecules coordinated to octahedral Mn, Co and Cu magnetic centres with short Cl…Cl contacts between them. The hydrazinium containing compounds are discrete complexes with magnetic coupling mediated by short Cl…Cl contacts while edge-sharing chains in the methylhydroxylamine phase are anticipated to dominate magnetic coupling. Magnetic property measurements for the four phases made in pure form show that all feature antiferromagnetic coupling. $Co(NH_3NH_2)_2(H_2O)_2Cl_4$ and $Cu(NH_2OCH_3)_2Cl_2$ are particularly interesting since the former shows clear evidence of strong magnetic frustration while the

[a] School of Physical Science, Ingram Building, University of Kent, Canterbury Kent, CT2 7NH, United Kingdom

Electronic Supplementary Information (ESI) available: CIFs from single crystal X-ray structure determination (also deposited in the CSD at entries 1877363-1877367) and figures displaying further crystallographic details, infrared spectra, magnetic property measurements, powder diffraction patterns, and thermogravimetric analysis are available. See DOI: 10.1039/x0xx00000x

later has magnetic properties that resemble a spin ½ 1D chain. This highlights the potential of these and related phases as hosts for low dimensional and frustrated magnetism.

2. Experimental Method

The four hydrazinium phases were made by slow evaporation of 20 mL solutions of $MnCl_2{\cdot}4H_2O$ (Acros Organics, 99+ %) or $CoCl_2{\cdot}6H_2O$ (Acros Organics, analytical grade) and NH_3NH_2Cl (Acros Organics, 98 %) over the course of 1-2 weeks at ambient temperature with quantitative yield. The solvent used was a 10:1 mixture of methanol:water, unless otherwise noted. Attempts to make Cu containing phases using $CuCl_2{\cdot}2H_2O$ (Sigma-Aldrich, ACS reagent 99%) were also made but were unsuccessful, leading to only physical mixtures of the reagents. $Co(NH_3NH_2)_2(H_2O)_2Cl_4$, hereafter known as **$Hyd_2CoCl_4$**, was made from the evaporation of a 0.091 M NH_3NH_2Cl and 0.046 M $CoCl_2{\cdot}6H_2O$ solution, resulting in the formation of pink blade crystals suitable for X-ray diffraction. Colourless block crystals of $(NH_3NH_2)_2Mn(NH_3NH_2)Cl_5$, referred to as **$Hyd_3MnCl_5$**, were made from the evaporation of a methanol solution containing 0.050 M NH_3NH_2Cl and 0.017 M $MnCl_2{\cdot}4H_2O$. Colourless block crystals of $Mn(NH_3NH_2)(H_2O)_2Cl_3$, known as **$HydMnCl_3$**, were made by evaporation of a 0.091 M NH_3NH_2Cl and 0.091 M $MnCl_2{\cdot}4H_2O$ solution. A sample of $(NH_3NH_2)_8Mn_3(NH_3NH_2)_2(H_2O)_2Cl_{16}$, **$Hyd_{10}Mn_3Cl_{16}$**, suitable for structural determination was made by evaporation of a 0.091 M NH_3NH_2Cl and 0.027 M $MnCl_2{\cdot}4H_2O$ solution, although a purer sample, which was used for bulk analysis, was obtained using 0.092 M NH_3NH_2Cl and 0.027 M $MnCl_2{\cdot}4H_2O$. In contrast $Cu(NH_2OCH_3)_2Cl_2$, referred to as **MHA_2CuCl_2**, was initially made by layering 8 mL of a 0.050 M methanol solution of $CuCl_2{\cdot}2H_2O$ over 8 mL of a 0.213 M $Na(HCO_2)$ and $(NH_3OCH_3)Cl$ solution in methanol:water (~12:1) leading to observing diffraction quality blue needle single crystals after a week. A larger sample for bulk property measurements was made by the same method by using 0.677 M $Na(HCO_2)$ and 0.427 M $(NH_3OCH_3)Cl$ methanol:water (~6:1) solution and 0.100 M $CuCl_2{\cdot}2H_2O$ solution in methanol, giving a good yield of 74.3 %. Similar reactions using $MnCl_2{\cdot}4H_2O$ lead to $NaMn(HCO_2)_3$ formation.[13]

Structure determinations were carried out using a Rigaku Oxford Diffraction Supernova equipped with MoK_α and Cu K_α microfocus sources (50 kV, 0.8 mA) with multi-layered focusing optics and an Atlas S2 CCD detector. Samples were held on MiTeGen microloops and, where needed, samples were cooled using an Oxford Cryosystems cryostream. Data were integrated and absorption corrections performed using CrysAlis Pro software suite version 171.38.46[14] and the structure solved using direct methods in SHELXT[15] and least-square refinements carried out using SHELXL-2014/7[16] via the Olex[2] graphical user interface[17] (see Table 1 for crystallographic details). Displacement parameters of non-hydrogen atoms were refined anisotropically. Hydrogen atom positions were typically located geometrically with displacement parameters constrained to 1.2 times the Ueq of the parent atoms (1.5 times for methyl groups and water molecules). Hydrogen bonding networks between discrete complexes are briefly discussed in the ESI.

Table 1: Crystallographic data for the structures determined in this work by single crystal X-ray diffraction.

Compound	**Hyd_2CoCl_4**	**Hyd_3MnCl_5**	**$HydMnCl_3$**	**$Hyd_{10}MnCl_{16}$**	**MHA_2CuCl_2**
Formula	$Co\,Cl_4\,H_{14}\,N_4\,O_2$	$Mn\,Cl_5\,H_{15}\,N_6$	$Mn\,Cl_3\,H_9\,N_2\,O_2$	$Mn_3\,Cl_{16}\,H_{54}\,N_{20}\,O_2$	$Cu\,Cl_2\,C_2\,H_{10}\,N_2\,O_2$
Formula Weight	302.88	331.37	230.38	1098.65	228.56
T (K)	293(2)	293 (2)	293(2)	293(2)	150(2)
λ (Å)	0.71073	0.71073	1.54184	1.54184	1.54184
Crystal System	Monoclinic	Monoclinic	Monoclinic	Triclinic	Triclinic
Space Group	$P2_1/c$	$P2_1/n$	$P2_1/n$	$P\bar{1}$	$P\bar{1}$
a (Å)	7.9880(6)	8.9779(4)	5.54110(10)	7.5839(3)	3.7868(6)
b (Å)	5.7019(5)	10.9705(4)	13.9707(3)	9.1752(4)	5.6827(9)
c (Å)	11.3808(8)	11.7726(5)	9.9630(3)	15.0656(6)	8.7079(11)
α (°)	90	90	90	89.821(4)	99.853(12)
β (°)	97.745(7)	94.423(4)	92.648(2)	84.447(3)	98.563(12)
γ (°)	90	90	90	75.697(4)	91.568(13)
V (Å^3)	513.63(7)	1156.05(9)	770.44(3)	1010.83(7)	182.30(5)
Z	2	4	4	1	1
ρ_{cal} (g cm^{-3})	1.958	1.904	1.986	1.805	2.082
μ (cm^{-1})	2.677	2.262	22.989	17.584	10.472
Refl. meas./unique	2489/1236 [R_{int} = 0.0311]	10289/2878 [R_{int} = 0.0237]	2816/1486 [R_{int} = 0.0258]	6591/3911 [R_{int} = 0.0292]	3563/759 [R_{int} = 0.0491]
Parameters refined	54	114	76	217	44
R_1, wR_2 (all)	0.0429, 0.0602	0.0403, 0.0801	0.0297, 0.0688	0.0341, 0.0818	0.0331, 0.0844
R_1, wR_2 (obs)	0.0311, 0.0548	0.0323, 0.0757	0.0270, 0.0660	0.0316, 0.0795	0.0314, 0.0806
Goodness of Fit	1.050	1.044	1.065	1.050	1.096

Journal Name

ARTICLE

Sample phase purity was established by powder X-ray diffraction using either a Rigaku Miniflex utilising Cu K_α radiation (40 kV, 15 mA) and a D/tex Ultra detector. Patterns were held in a plastic sample holder with a 10 mm well, due to these products often reacting with other holders to which they are exposed for a prolonged time, with data typically collected over a range of 5-60° 2θ. The data obtained were subsequently fitted using the Le Bail method in the program Rietica,[18] which indicated that the bulk samples were consistent with the crystal structures of the phases determined by single crystal X-ray diffraction and were either single phase or contained trace quantities of this phase (see Fig. S1-4). **Hyd_3MnCl_5** was an exception to this and always contained significant quantities of unidentified phases that prevented further characterisation of this compound. Elemental microanalysis, performed at the London Metropolitan University, confirmed the purity of the four other samples. **Hyd_2CoCl_4** was found to be 4.61 % H and 18.40 % N *c.f.* to 4.66 % H and 18.38 % expected. **$HydMnCl_3$** consisted of 3.86 % H and 11.98 % N *c.f.* 3.94 % H and 12.16 % N expected. **$Hyd_{10}Mn_3Cl_{16}$** was comprised of 5.03 % H and 25.36 % N *c.f.* 4.95 % H and 25.50 % N. **MHA_2CuCl_2** was found to be 10.36 % C, 4.35 % H and 12.01 % N *c.f.* 10.51 % C, 4.41 % H and 12.26 % N expected.

Magnetic properties of the four phases prepared in high purity were analysed by a Quantum Design MPMS 5 magnetometer using a 7 T superconducting magnet. Samples were placed in gelatin capsules inside a pierced straw with a uniform diamagnetic background. Thermal stabilities of the same samples were analysed using a NETZSCH 409 PG/PC TGA with simultaneous DSC capabilities. The sample was held in an alumina crucible under flowing air and typically heated at a rate of 10°/minute to 800 °C, with the exception of **MHA_2CuCl_2** where a heating rate of 5°/minute was used due to the high exothermic nature of its initial decomposition. Infrared spectra were collected over a range of 4000-500 cm^{-1} using a Shimadzu IRAffinity-1S Fourier transform spectrometer equipped with an attenuated total reflection stage (see ESI for spectra, Fig. S5-8, and their assignments); measurements were averaged over a total of 16 scans.

3. Results and Discussion

3.1 Crystal Structures

Hyd_2CoCl_4 adopts $P2_1/c$ monoclinic symmetry with discrete octahedral Co complexes. The asymmetric unit of **Hyd_2CoCl_4** contains one Co atom, on an inversion centre, an H_2O and a NH_3NH_2 ligand and two Cl atoms, one of which is coordinated to the Co (see Fig. S9). The Co atoms are coordinated to N atoms from two hydrazinium cations, two oxygen atoms from water molecules and two chloride anions, with like atoms bound in a *trans*-fashion. The bond valence sum of Co is 1.94, consistent with a divalent cation.[19] The relatively regular octahedral Co cations are connected by Cl…Cl contacts (3.7413(11) Å) into a layer with Co in a diamond-like arrangement (see Fig. 1). The space between these layers is occupied by an undulating layer of Cl anions, with nearest intralayer and interlayer Cl…Cl contacts of 3.827(4) and 3.8191(10) Å. Neighbouring Co cations in a diamond all have the same Co-Cl…Cl-Co contacts with a likely magnetic exchange pathway of 8.5522(15) Å and a dihedral angle of 127.49(2)°. It should, however, be noted that the distance separating the closest two Co cation on opposite sides of the diamond are shorter than those bridged by the Cl…Cl contacts (*c.f.* 5.7016(5) to 6.3642(4) Å). All Cl…Cl contacts between layers involve three Cl atoms so coupling between layers must be far weaker; the nearest-neighbour Co-Co distance between layers is also much longer (*c.f.* 7.9862(6) to 5.7017(5) Å).

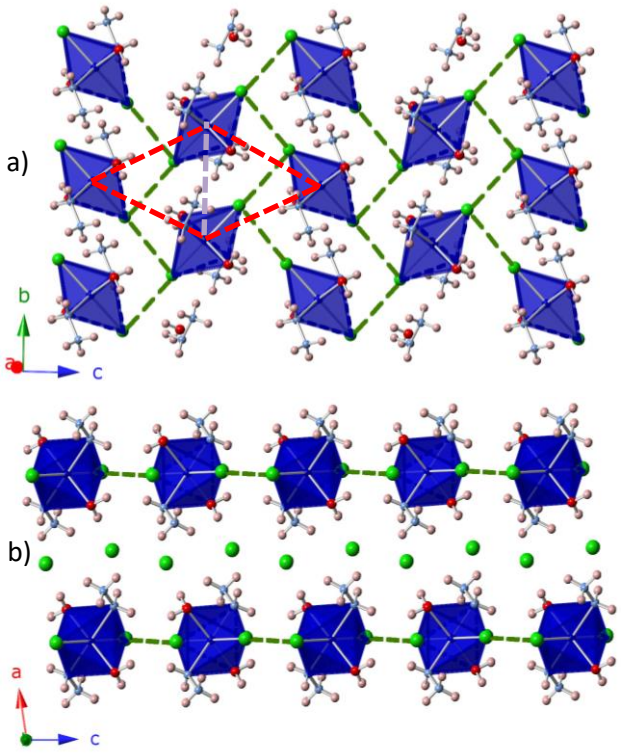

Fig. 1: Crystal structure of **Hyd_2CoCl_4** showing a) the structure of an individual layer and b) the arrangement of neighbouring layers. The Co octahedra are shown in dark blue and Cl, C, N, O and H atoms are shown as dark green, black, light blue, red and light pink spheres, respectively. Nearest neighbour Cl…Cl contacts within a layer are shown as dashed lines. The Co centres in one diamond are highlighted in Fig. 1a by red dashed lines and the nearest neighbours through space highlighted by a lavender dashed line.

Hyd_3MnCl_5 adopts $P2_1/n$ monoclinic symmetry and consists of relatively regular discrete octahedral complexes. The asymmetric unit contains one Mn atom, five Cl atoms, one complete NH_3NH_2 ligand and two complete uncoordinated $NH_3NH_2^+$ cations (see Fig. S10). The Mn atom is coordinated to five Cl atoms and one NH_3NH_2 ligand and has a bond valence sum of 1.95, consistent with Mn^{2+}.[19] The shortest Cl…Cl contacts, of 3.718(6) Å, between molecular complexes connect these into chains that run roughly along the [101] axis, while modestly longer Cl…Cl contacts, 3.879(2) to 3.918(2) Å connect complexes within the *ab* plane into an approximately square lattice, completing a three dimensional network (see Fig. 2).

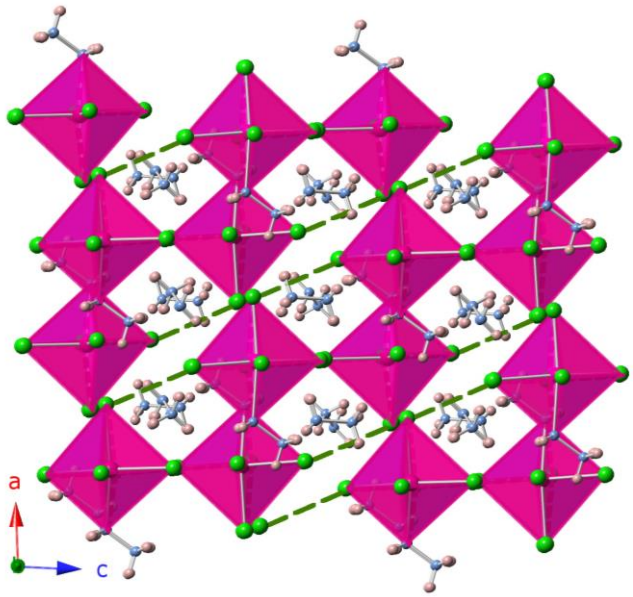

Fig. 2: Crystal structure of **Hyd_3MnCl_5** showing Mn-Cl…Cl-Mn chains. The Mn octahedra are shown in pink and all other colours are the same as Fig. 1.

$HydMnCl_3$ adopts $P2_1/n$ monoclinic symmetry in which the Mn atoms are in molecular octahedral complexes, with relatively regular geometry. The asymmetric unit of **$HydMnCl_3$** features one Mn atoms, a complete hydrazinium, two complete water molecules and three chloride atoms, all on general positions (see Fig. S11). In these complexes the Mn is coordinated to a N atom from a NH_3NH_2 ligand, the oxygen atoms from the two distinct two water molecules in *cis*-positions and three Cl atoms, in a *fac*-fashion. The bond valence sum of the Mn cation is 2.05, consistent with Mn^{2+}.[19] The **$HydMnCl_3$** complexes are connected by an intricate network of Cl…Cl contacts (see Fig. 3). The shortest of these form zig-zag chains along the *a*-axis with alternating contacts of 3.515(3) and 3.771(3) Å (see Fig. S12). Other zig-zag chains of **$HydMnCl_3$** complexes are formed by alternating contacts of 3.895(4) and 3.982(4) Å; these two types of zig-zag chains are interconnected into undulating layers along the *ac* plane. The likely superexchange pathways are through Mn-Cl…Cl-Mn contacts which occur in all three dimensions, with distances of 8.452(4) and 8.708(4) Å in the zig-zag chains with the shortest Cl…Cl contacts, these have dihedral angles of 180°. The longer Cl…Cl contacts lead to much longer exchange pathways of at least 8.890(5) Å with much smaller dihedral angles of 47.72(2)° and 62.11(2)°.

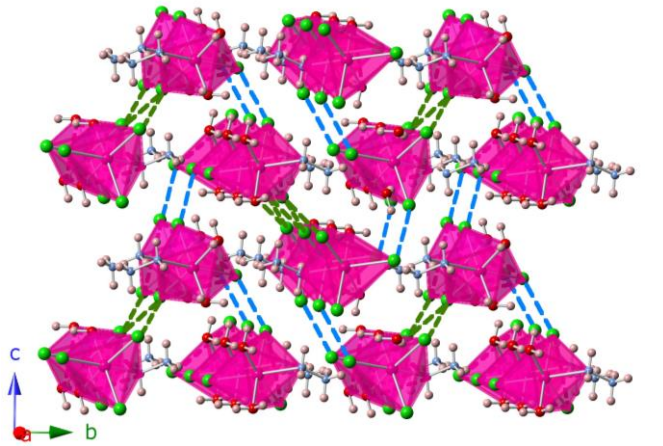

Fig. 3: Crystal structure of **$HydMnCl_3$** showing the two sets of zig-zag Mn-Cl…Cl-Mn chains with the closest Cl…Cl contacts shown as green dashed lines and the Cl…Cl contacts in the other chain shown in blue. The Mn octahedra are shown in pink and all other colours are the same as in Fig. 1.

$Hyd_{10}Mn_3Cl_{16}$ adopts $P\bar{1}$ triclinic symmetry and features two distinct Mn octahedral complexes. The asymmetric unit contains 2 Mn atoms, with Mn1 found on an inversion centre, one H_2O, five NH_3NH_2 molecules and eight distinct Cl atoms (see Fig. S13). Mn1 is coordinated to six Cl atoms generated from three crystallographic distinct positions while Mn2 is coordinated to four Cl atoms, one NH_3NH_2 ligand and a H_2O molecule, with the molecular ligands bound in a *cis*-fashion. The bond valence sums of the Mn cations are 1.85 and 2.02 for Mn1 and Mn2, respectively, broadly consistent with Mn^{2+}.[19] The structure of **$Hyd_{10}Mn_3Cl_{16}$** can be viewed as layers of regular octahedral Mn complexes stacked along the *c*-axis that only contain Mn1 or Mn2 atoms, with the following sequence: Mn1Mn2Mn2Mn1 (see Fig. 4). While the octahedral Mn2 centres in neighbouring layers are stacked on top of each other, $Mn1Cl_6$ octahedra are shifted by about half a unit cell along both the *a*- and *b*-axis compared to the octahedral Mn2 centres in the layers above and below it. $NH_3NH_2^+$ cations and Cl^- anions occupy space between the octahedral Mn2 centres in a layer. Short Cl…Cl contacts (3.712(7) and 3.798(9) Å) connect Mn1 atoms to Mn2 atoms in the layer above and below, forming rhombohedra that are linked to each other by their corners (see Fig. S14 for more details of Cl…Cl contact distances). The only other Cl…Cl contacts of comparable length (3.775(3) Å) are between these free Cl^- anions and Cl atoms coordinated to Mn2. Longer Cl…Cl links crosslink the neighbouring rhombohedra (3.9464(17) Å) and Mn2 cations are connected by Cl…Cl interactions of similar lengths both within (3.946(11) Å) and between the layers (3.980(6) Å). The shortest potential magnetic coupling pathways alternate within the rhombohedra with distances of 8.809(9) Å and 8.902(11) Å distances and dihedral angles of 69.40(2) and 127.353(15)°. The exchange pathways associated with the other Cl...Cl contacts mentioned above are between 8.951(13) and 9.024(6) Å long with generally have smaller dihedral angles, between 27.30(3) and 84.15(2)°.

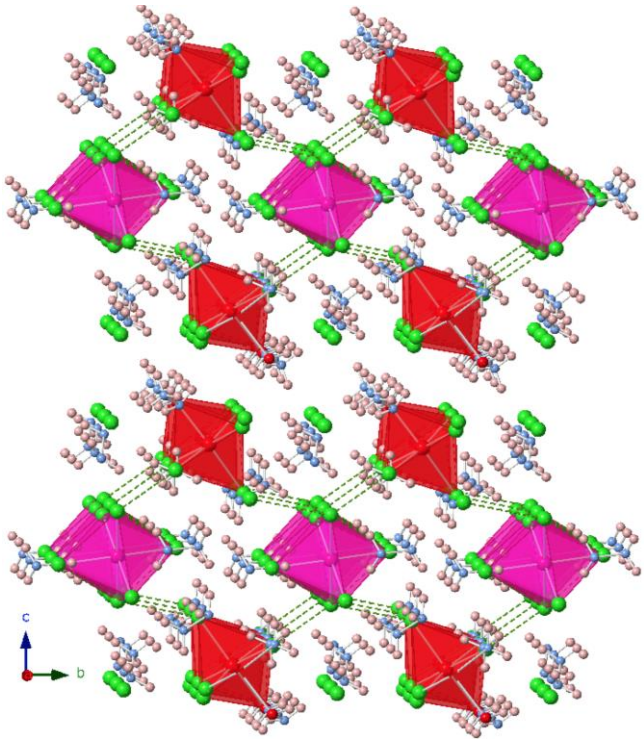

Fig. 4: Structure of $\mathbf{Hyd_{10}Mn_3Cl_{16}}$ showing the rhombohedral arrangements of octahedra connected by short Cl…Cl contacts. The Mn1 and Mn2 octahedra are pink and red and all other colours are as in Fig. 1.

Unlike the other phases in this article $\mathbf{MHA_2CuCl_2}$, which adopts $P\bar{1}$ triclinic symmetry, contains 1D chains of Cu connected by Cl atoms. The asymmetric unit of $\mathbf{MHA_2CuCl_2}$ features one Cu atom, on a special position with half the site multiplicity of the general position, one O-MHA ligand and one Cl ligand (see Fig. S15). The Cu cations are coordinated to the N atoms of two O-MHA ligands, in a *trans*-fashion, and four Cl ligands; the Jahn-Teller distortion significantly elongates two of the Cu-Cl bonds (*c.f.* 2.312(20) Å to 2.866(19) Å). The bond valence sum of the Cu cation is 2.06, consistent with a divalent Cu cation.[19] The octahedral Cu are arranged in edge-sharing chains bridged through Cl ligands with close Cl…Cl contacts (3.820(19) Å) between chains connecting these into a layer, which are well separated from each other by the bulk of the O-MHA ligand that interdigitate between layers (see Fig. 5). With regards to potential magnetic coupling within the chains the Jahn-Teller axis of the Cu alternates so that the intrachain super-exchange bridges all involve a long and a short Cu-Cl bond, leading to a super-exchange distance of 5.18(3) Å and a Cu-Cl-Cu bond angle of 93.38(4)°. The magnetic coupling between chains in a layer is likely to be facilitated through Cu-Cl…Cl-Cu pathways, which are 8.44(3) Å and a dihedral angle of 180°. Between the layers only through-space interactions are possible, which are likely to be very weak due to the 8.7078(11) Å nearest neighbour distances between Cu in neighbouring planes, which are also far longer than nearest neighbour Cu distances within the layers (3.787(6) Å and 5.6824(9) Å, respectively).

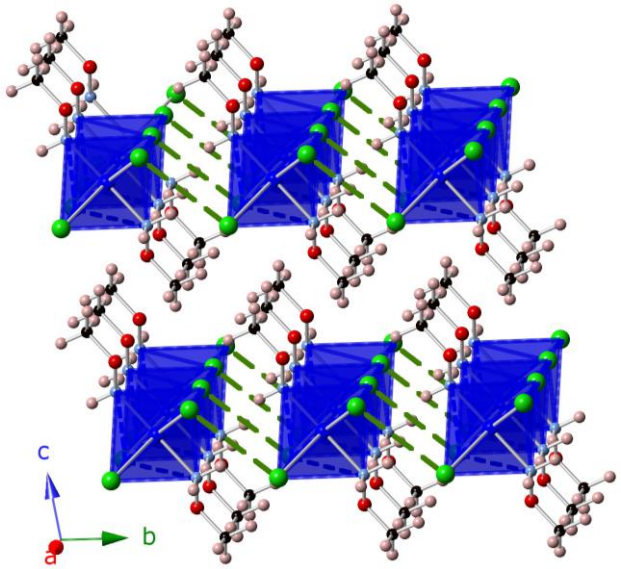

Fig. 5: Crystal structure of $\mathbf{MHA_2CuCl_2}$ showing the structure viewed along the edge-sharing chains. The Cu octahedra are shown in dark blue and all other colours are the same as Fig. 1.

3.2 Thermal Stability

Thermogravimetric analysis indicated that $\mathbf{Hyd_2CoCl_4}$ is stable in air until 80 °C where mass corresponding to the two water molecules is lost in an endothermic process (see Fig. S16). Further mass loss is then observed between 165 °C and 360 °C, with the product at this stage likely $CoCl_2$ based on the residual mass; this stage of the decomposition appears to be a two stage process with the first half endothermic and the second half exothermic. This may suggest that chloride is lost first and then NH_2NH_2 molecules during the second stage of the process since decomposition of the later is highly exothermic. The final stage of decomposition takes place between 470 and 660 °C via a mildly exothermic process, with the final mass of the residue confirmed by powder X-ray diffraction to be Co_3O_4.

$\mathbf{HydMnCl_3}$ appears to be stable to only 50 °C above which mass broadly corresponding to losing its water molecules occurs in an endothermic process (see Fig. S17). This anhydrous phase is then stable until 275 °C above which weight is lost in a two stage process which finishes at 700 °C; the final product from this decomposition process has been identified to be a mixture of Mn_3O_4 and Mn_2O_3 by powder X-ray diffraction.

$\mathbf{Hyd_{10}Mn_3Cl_{16}}$ initially decomposes between 60 and 100 °C in an endothermic process consistent with the loss of the water molecules (see Fig. S18). This anhydrous phase is then stable to 170 °C above which mass is lost continually up to 625 °C, where residual mass is consistent with the formation of Mn_2O_3, confirmed by powder X-ray diffraction. There is a clear change in slope of weight loss between a rapid decrease to a much more gradual decrease at around 360 °C, with the process below this being high exothermic and only mildly so above this temperature.

$\mathbf{MHA_2CuCl_2}$ is stable up to 100 °C in air where it undergoes a highly exothermic decomposition in a single rapid step that is

complete by 150 °C and involves loosing mass equivalent to the organic ligands (see Fig. S19). Almost continuous mass loss is observed above this temperature up to 500 °C via mildly exothermic processes, yielding a final product confirmed by powder X-ray diffraction to be CuO.

3.3 Magnetic Properties

Magnetic susceptibility measurements (χ) of **Hyd_2CoCl_4** obtained in an applied field of 1000 Oe increase gradually on cooling with field cooled (FC) measurements and zero field cooled (ZFC) measurements not diverging, indicating the phase remains paramagnetic down to 1.8 K (see Fig. 6). χ can be fit between 75-300 K using Curie-Weiss law yielding a Curie-Weiss temperature, Θ_{CW}, of -18.75 K, indicating moderate antiferromagnetic coupling, and an effective magnetic moment of 4.95 μ_B; this is within the range of typical values exhibited by octahedral Co^{2+} and is consistent with the orbital angular momentum not being fully quenched.[20] At 300 K, χT is 2.89 emu K mol^{-1} Oe^{-1}; this gradually decreases to 100 K before falling rapidly below this to 1.75 emu K mol^{-1} Oe^{-1} around 5 K (see Fig. S20), consistent with significant antiferromagnetic coupling at low temperature. While isothermal magnetisation measurements at 1.8 K are also consistent with paramagnetic behaviour, increasingly linearly at low applied fields before saturating near 24 kOe, the value of 2.2 μ_B per magnetic centre observed at 50 kOe is around half the value typically expected for Co^{2+} (see Fig. S21). This is likely the result of significant local antiferromagnetic interactions in this phase at low temperature despite long-range magnetic order being supressed by magnetic frustration. This is consistent with a frustration index $|\Theta_{CW}/T_N|$, where T_N is the Néel temperature, of at least 11.2. The cause of this magnetic frustration is unclear as antiferromagnetic interactions within the diamonoid layers of Co atoms are not frustrated if only nearest neighbours coupled through Co-Cl…Cl-Co bridges are considered, which are anticipated to be the dominant magnetic coupling pathways in this compound. Geometrically the most likely source of magnetic frustration is competition between antiferromagnetic coupling through Co-Cl…Cl-Co bridges in the diamond and between nearest neighbouring Co cations in space, which are formally on the opposite sides of the diamond. While the later are far enough apart in space, 5.7016(5) Å, that direct exchange seems unlikely the magnetic coupling between these may be facilitated by Co-Cl…Cl…Cl-Co contacts (a total exchange pathway of 12.2932(18) Å) or coupling via a Co-Cl…O-Co pathway (with a total exchange pathway of 7.860(6) Å).

□□e χ □□ **$HydMnCl_3$** and **$Hyd_{10}Mn_3Cl_{16}$** continually increase at low temperatures and show no indication of divergence of ZFC and FC measurements, consistent with both compounds remaining paramagnetic down to the lowest temperature examined (see Fig. S22 and Fig. S23). In both cases χ can be fit by Curie-Weiss law across the whole temperature range examined, 1.8-300 K, yielding a Θ_{CW} of -2.6 K and -0.9 K, for **$HydMnCl_3$** and **$Hyd_{10}Mn_3Cl_{16}$** indicative of weak antiferromagnetic coupling in both compounds (see Fig. S22 and Fig. S23). Effective magnetic moments of 5.77 μ_B obtained for both **$HydMnCl_3$** and **$Hyd_{10}Mn_3Cl_{16}$**, close to the 5.92 μ_B expected for spin-only Mn^{2+}. For **$HydMnCl_3$** a χ□ value of 4.14 emu K mol^{-1} Oe^{-1} is observed at 300 K, consistent with isolated Mn^{2+} centres, with this remaining nearly constant to 80 K. Below this temperature a rapid decrease is observed to values approaching 1.5 emu K mol^{-1} Oe^{-1} at 1.8 K, consistent with the emergence of short range antiferromagnetic coupling (see Fig. S24). The χT behaviour of **$Hyd_{10}Mn_3Cl_{16}$** is similar with a value of 4.14 emu K mol^{-1} Oe^{-1} also observed at 300 K, which remains relatively constant until 50 K before falling rapidly to about 2.4 emu K mol^{-1} Oe^{-1} at 1.8 K (see Fig. S24). This suggests the antiferromagnetic coupling in **$Hyd_{10}Mn_3Cl_{16}$** is weaker than in **$HydMnCl_3$**, consistent with their respective Θ_{CW}. Isothermal magnetisation measurements at 1.8 K of both compounds increase linearly up to fields of about 20 kOe before beginning to saturate, reaching a value of 4.2 and 4.8 μ_B per Mn^{2+} atom at 50 kOe, for **$HydMnCl_3$** and **$Hyd_{10}Mn_3Cl_{16}$**, consistent with paramagnetic behaviour (see Fig. S25).

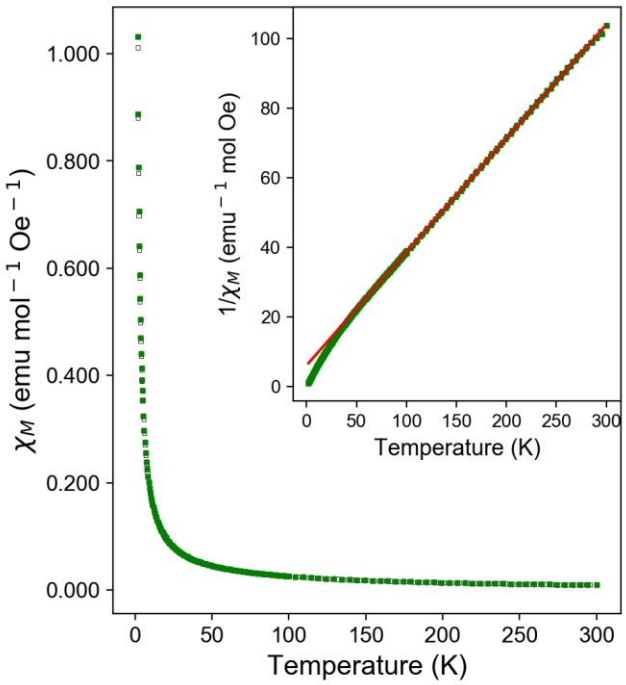

Fig. 6: Evolution of χ versus temperature from 1000 Oe ZFC (hollow black symbol) and FC (filled green symbol) measurements for **Hyd_2CoCl_4**. The insert shows a Curie-Weiss fit (red line) to the inverse susceptibility from 75-300 K.

χ measurements of **MHA_2CuCl_2** feature a broad cusp, indicating the emergence of antiferromagnetic order below 29 K, with the width of this feature suggestive of low dimensional magnetic order (see Fig. 7). Below 5 K the magnetic susceptibility decreases at an increasing rate, suggesting the possibility of another magnetic transition. Tiny increases in magnetic susceptibility below 2.5 K may be indicative of a small paramagnetic impurity. χ measurements obtained in an applied field of 1000 Oe can be fit over the range of 70-300 K using Curie-Weiss law, yielding a Curie-Weiss temperature of -28.3 K, consistent with moderate antiferromagnetic coupling, and an effective magnetic moment of 1.77 μ_B, close to the

expected spin-only value of 1.73 μ_B expected for Cu^{2+} (see Fig. S26). A plot of χT indicates a value of 0.36 emu K mol^{-1} Oe^{-1}, close to that expected for isolated Cu^{2+} centres and that this drops rapidly below 100 K approaching towards zero at 1.8 K, consistent with the emergence of antiferromagnetic interactions (see Fig. S27). Isothermal magnetisation measurements at 1.8 K, 2.8 K and 10 K are very similar with slow linear increases in magnetisation observed to just over 0.04 μ_B per Cu^{2+} under an applied field of 50 kOe, consistent with antiferromagnetic order (see Fig. S28).

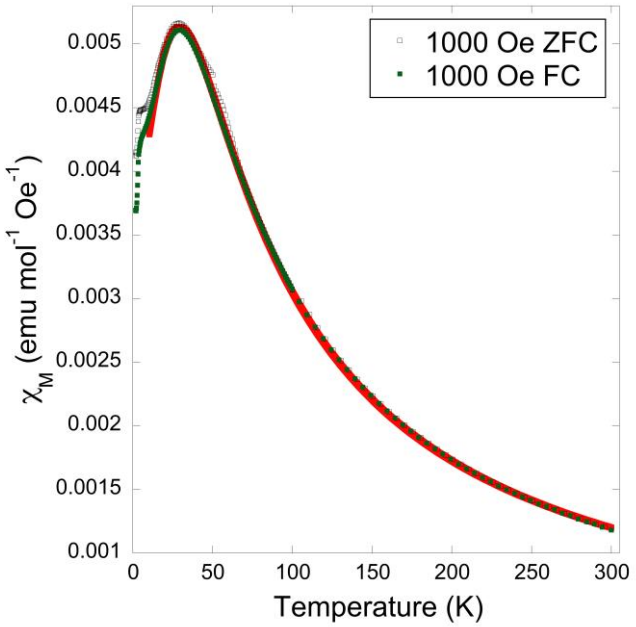

Fig. 7: Evolution of χ versus temperature from 1000 Oe ZFC (hollow symbol) and FC (filled symbol) measurements with a red line showing a spin ½ Heisenberg chain fit to the FC data.

Given the anticipation that the magnetic interactions within the chains in **MHA_2CuCl_2** should be dominant we attempted to fit the evolution of χ with temperature with the well-known Bonner-Fisher approximation for a spin ½ Heisenberg chain,[21] which takes the formulism:

$$\chi = \frac{N_A g^2 \mu_B^2}{k_B T} \times \frac{0.25 + 0.074975x + 0.075236x^2}{1 + 0.9931x + 0.172135x^2 + 0.757825x^3}$$

where $x = |J|/k_B T$. Excellent fits to both ZFC and FC data collected at 1000 Oe above 10 K were obtained yielding values within two standard deviations of each other; with those to the FC data giving g = 2.0547(15) and J/k_B = 45.26(8) K (see Fig. 7). This suggests that **MHA_2CuCl_2** is predominantly a 1D antiferromagnet, although as indicated, for example,[22] by our previous paper on 1D formate frameworks this does not exclude the presence of significant interchain coupling, particularly through the Cl…Cl close contacts in the plane.

It is difficult to compare the magnetic behaviour of four compounds with significant differences in topologies and containing distinct magnetic cations. The different strengths of the magnetic interactions, as measured by Θ_{CW}, however can be rationalised with regards to the length of the likely exchange pathways in these compounds. **MHA_2CuCl_2**, which appears to predominantly have coupling within its edge-sharing chains has the highest Θ_{CW}. This is followed by **Hyd_2CoCl_4**, which is connected within a layer by relatively short 8.552(15) Å Co-Cl…Cl-Co pathways. Both **$HydMnCl_3$** and **$Hyd_{10}Mn_3Cl_{16}$** have much lower Θ_{CW}, and while their precise topology undoubtedly play a significant role in this, it is notable that these compound require Mn-Cl…Cl-Mn contacts of 8.708(4) and 8.809 (9) Å to connect the octahedral centres into extended units, with the later having the weaker Θ_{CW} of the two. Comparison to a number of previously reported compounds with coupling mediated by Cl…Cl contacts into an extended unit, most typically chains in $AMCl_4$ (where A is an organic cation and B is typically Cu) type compounds, suggests that for magnetic order to emerge above 1.8 K typically the Cl…Cl contact must be less than 3.9 Å.[6, 11, 23] This is consistent with the emergence of magnetic order in **MHA_2CuCl_2** and **Hyd_2CoCl_4** while the lack of magnetic order from **$HydMnCl_3$** and **$Hyd_{10}Mn_3Cl_{16}$** despite Cl…Cl contacts in this range may be a result of the precise architectures of these compounds, including the specific bond and dihedral angles, which are also known to have a significant effect on magnetic coupling.[8]

Conclusions

This study has reported the synthesis, crystal structures and magnetic properties of five octahedral Mn, Co and Cu complexes with simple amine ligands. Despite adopting a wide variety of crystal structures they all exhibit close Cl…Cl contacts, which in the majority of cases are the principle source of magnetic coupling. The four compounds whose magnetic properties are measured all show antiferromagnetic interactions. While in **$HydMnCl_3$** and **$Hyd_{10}Mn_3Cl_{16}$** these are relatively weak **Hyd_2CoCl_4** and **MHA_2CuCl_2** exhibit significant magnetic coupling. There is no indication of magnetic order emerging in **Hyd_2CoCl_4** above 1.8 K indicating that this compound is likely highly magnetically frustrated, with an analysis of its crystal structure showing this is likely restricted to the diamonoid layers of Co cations. In contrast **MHA_2CuCl_2** exhibits magnetic susceptibility measurements which are well fitted by a 1D spin ½ Heisenberg antiferromagnetic model, with this coupling likely facilitated by Cl^- bridges that link octahedra in an edge-sharing fashion.

Conflicts of interest

There are no conflicts of interest to declare.

Acknowledgements

The authors would like to thank EPSRC for funding as part of grant EP/R011524/1. One of us (RJCD) would like to thank for the University of Kent for funding via a Vice-Chancellors PhD studentship.

References

1 a) B. J. Kim, H. Koh, E. Rotenberg, S. J. Oh, H. Eisaki, N. Motoyama, S. Uchida, T. Tohyama, S. Maekawa, Z. X. Shen and C. Kim, *Nat. Phys.*, 2006, **2**, 397-401; b) L. S. Wu, W. J. Gannon, I. A. Zaliznyak, A. M. Tsvelik, M. Brockmann, J. S. Caux, M. S. Kim, Y. Qiu, J. R. D. Copley, G. Ehlers, A. Podlesnyak and M. C. Aronson, *Science*, 2016, **352**, 1206-1210.

2 a) T. Koretsune and M. Ogata, *Phys. Rev. Lett.*, 2002, **89**, 116401; b) M. V. Chandra, *Rep. Prog. Phys.*, 2016, **79**, 082501.

3 a) A. P. Ramirez, *Annu. Rev. Mater. Sci.*, 1994, **24**, 453-480; b) R. Moessner and A. P. Ramirez, *Physics Today*, 2006, **59**, 24-29.

4 L. C. Chapon, *Phys. Rev. B*, 2009, **80**, 172405.

5 a) Y.-G. Huang, F.-L. Jiang and M.-C. Hong, *Coord. Chem. Rev.*, 2009, **253**, 2814-2834; b) P. Canepa, Y. J. Chabal and T. Thonhauser, *Phys. Rev. B*, 2013, **87**, 094407; c) P. J. Saines and N. C. Bristowe, *Dalton Trans.*, 2018, **47**, 13257-13280.

6 F. Awwadi, R. D. Willett, B. Twamley, R. Schneider and C. P. Landee, *Inorg. Chem.*, 2008, **47**, 9327-9332.

7 a) A. Shapiro, C. P. Landee, M. M. Turnbull, J. Jornet, M. Deumal, J. J. Novoa, M. A. Robb and W. Lewis, *J. Am. Chem. Soc.*, 2007, **129**, 952-959; b) D. Schmidiger, P. Bouillot, T. Guidi, R. Bewley, C. Kollath, T. Giamarchi and A. Zheludev, *Phys. Rev. Lett.*, 2013, **111**, 107202.

8 C. P. Landee and M. M. Turnbull, *Eur. J. Inorg. Chem.*, 2013, **2013**, 2266-2285.

9 a) P. J. Saines, M. Steinmann, J.-C. Tan, W. Li, P. T. Barton and A. K. Cheetham, *Inorg. Chem.*, 2012, **51**, 11198-11209; b) P. J. Saines, P. T. Barton, M. Jura, K. S. Knight and A. K. Cheetham, *Mater. Horiz.*, 2014, **1**, 332-337; c) P. J. Saines, J. A. M. Paddison, P. M. M. Thygesen and M. G. Tucker, *Mater. Horiz.*, 2015, **2**, 528-535.

10 a) R. D. Willett, C. Galeriu, C. P. Landee, M. M. Turnbull and B. Twamley, *Inorg. Chem.*, 2004, **43**, 3804-3811; b) R. T. Butcher, M. M. Turnbull, C. P. Landee, A. Shapiro, F. Xiao, D. Garrett, W. T. Robinson and B. Twamley, *Inorg. Chem.*, 2010, **49**, 427-434.

11 M. Abdalrahman, C. P. Landee, S. G. Telfer, M. M. Turnbull and J. L. Wikaira, *Inorg. Chim. Acta*, 2012, **389**, 66-76.

12 a) N. K. Makmudova, N. A. Parpiev, Kh. T. Sharipov and S. S. Val'dman, *Uzb. Kim. Zh*, 1977, 57; b) O. S. Bushuyev, F. A. Arguelles, P. Brown, B. L. Weeks and L. J. Hope-Weeks, *Eur. J. Inorg. Chem.*, 2011, **2011**, 4622-4625.

13 a) V. Paredes-García, A. Vega, M. A. Novak, M. G. F. Vaz, D. A. Souza, D. Venegas-Yazigi and E. Spodine, *Inorg. Chem.*, 2009, **48**, 4737-4742; b) J. C. Aston and P. J. Saines, *Z. Anorg. Allg. Chem.*, 2017, **643**, 287-293.

14 *CrysAlis PRO* version 171.38.46, Rigaku, Culham, Oxfordshire, England, **2017**.

15 G. Sheldrick, *Acta Crystallogr. A*, 2015, **71**, 3-8.

16 G. Sheldrick, *Acta Crystallogr. C*, 2015, **71**, 3-8.

17 O. V. Dolomanov, L. J. Bourhis, R. J. Gildea, J. A. K. Howard and H. Puschmann, *J. Appl. Crystallogr.*, 2009, **42**, 339-341.

18 B. A. Hunter and C. J. Howard, *A computer program for Rietveld analysis of X-ray and neutron powder diffraction patterns,*, Lucas Heights Laboratories, 1998.

19 N. E. Brese and M. O'Keeffe, *Acta Crystallogr.*, 1991, **B47**, 192-197.

20 A. R. West, *Solid State Chemistry and Its Applications*, Wiley, Singapore, Second Edition edn., 2014.

21 J. C. Bonner and M. E. Fisher, *Phys. Rev.*, 1964, **135**, A640-A658.

22 S. M. Bovill, R. J. C. Dixey and P. J. Saines, *CrystEngComm*, 2017, **19**, 1831-1838.

23 a) G. W. Tremelling, B. M. Foxman, C. P. Landee, M. M. Turnbull and R. D. Willett, *Dalton Trans.*, 2009, 10518-10526; b) K. Edwards, S. N. Herringer, A. R. Parent, M. Provost, K. C. Shortsleeves, M. M. Turnbull and L. N. Dawe, *Inorg. Chim. Acta*, 2011, **368**, 141-151.